

The general trends predicted by the extension of equation (2.5) considering the states of both bands (g.b., s.b.) observed below and above the crossing may be qualitatively reasonably up to even high spin  $I^\pi \geq 28_s^+$ .

### III.2.2- - Method 2: VMI Predictions:-

In an attempt to obtain still better agreement with the experiment data, we have used equations (2.6, 2.8). Where  $\theta_0$  and C were determined for the ground state band below  $I_{\text{cross}}$ , they were substituted back in equation (2.6). The other two adjustable parameters of this model <sup>(12)</sup>,  $E_0$  and A, were determined for the super band and substituted in equation (2.8).

These two equations are solved for E corresponding to each value of I. it should be remember that the parameters  $\theta_0$ , C,  $E_0$ , A were determined so as to yield a best fit to the experimental energies. The values of the parameters obtained are listed in table (4).

The results obtained are listed in tables (5, 6) for (<sup>176-186</sup>Pt). The calculated energy levels are shown in figs (4-9) as compared with the observed energy levels for the chosen isotopes. A good agreement is shown.

It can be seen, in tables (5-6) that, the super band crosses the ground state band around spin  $14^+$  for <sup>176</sup>Pt and <sup>184</sup>Pt, while the super band crosses the ground state band around spin  $16^+$  for <sup>178</sup>Pt and <sup>182</sup>Pt, the super band crosses the ground state band around spin  $18^+$  for <sup>180</sup>Pt and  $12^+$  for <sup>186</sup>Pt.

This crossing may cause the backbending. The backbending phenomenon is currently interpreted as the band crossing of the ground state rotational band (g) and the spin aligned particle super band (s).

Especially  $i_{\frac{13}{2}}$  neutrons are considered to be responsible for the backbending in these nuclei due to the large Coriolis force <sup>(29)</sup>.

**Table (4).** The values of parameters  $\theta_0$ , C,  $E_0$ , A

The nucleus	$\theta_0$ (Mev) <sup>-1</sup>	C (Mev) <sup>-3</sup>	$E_0$ (Mev)	A (Mev)
<sup>176</sup> Pt	12.0	0.00107	1,290	0.00814
<sup>178</sup> Pt	15.6	0.00111	1,410	0.00793
<sup>180</sup> Pt	17.9	0.00150	1,638	0.00756
<sup>182</sup> Pt	15.6	0.00111	1,445	0.00780
<sup>184</sup> Pt	14.6	0.00107	1.178	0.00785
<sup>186</sup> Pt	10.2	0.00104	0.863	0.00933

**Table (5).** The experimental yrast levels in  $^{176}\text{Pt}$ ,  $^{178}\text{Pt}$  and  $^{180}\text{Pt}$  are given along with the calculated energies (method 2).

The nucleus $^{176}\text{Pt}$			The nucleus $^{178}\text{Pt}$			The nucleus $^{180}\text{Pt}$		
$I^\pi$	$E_{\text{ex}}$	$E_{\text{th2}}$	$I^\pi$	$E_{\text{ex}}$	$E_{\text{th2}}$	$I^\pi$	$E_{\text{ex}}$	$E_{\text{th2}}$
(g.b)			(g.b)			(g.b)		
$2^+$	0.264	0.184	$2^+$	0.170	0.159	$2^+$	0.153	0.149
$4^+$	0.564	0.489	$4^+$	0.427	0.442	$4^+$	0.411	0.432
$6^+$	0.906	0.870	$6^+$	0.765	0.804	$6^+$	0.757	0.805
$8^+$	1.306	1.307	$8^+$	1.178	1.226	$8^+$	1.182	1.246
$10^+$	1.765	1.791	$10^+$	1.661	1.696	$10^+$	1.675	1.741
$12^+$	2.277	2.314	$12^+$	2.209	2.207	$12^+$	2.229	2.283
$14^+$	2.833	2.872	$14^+$	2.814	2.754	$14^+$	2.842	2.867
			$16^+$	3.459	3.334	$16^+$	3.505	3.487
						$18^+$	4.252	4.141
(s.b)			(s.b)			(s.b)		
$16^+$	3.423	3.470	$18^+$	4.110	4.122	$20^+$	4.804	4.811
$18^+$	4.041	4.031	$20^+$	4.754	4.741	$22^+$	5.467	5.461
$20^+$	4.690	4.656	$22^+$	5.430	5.423	$24^+$	6.178	6.171
$22^+$	5.377	5.345	$24^+$	6.159	6.168	$26^+$	6.935	6.942
$24^+$	6.107	6.099						
$26^+$	6.879	6.916						

Method 2 is the variable moment of inertia (VMI)

**Table (6).** The experimental yrast levels in  $^{182}\text{Pt}$ ,  $^{184}\text{Pt}$  and  $^{186}\text{Pt}$  are given along with the calculated energies (method 2).

The nucleus $^{182}\text{Pt}$			The nucleus $^{184}\text{Pt}$			The nucleus $^{186}\text{Pt}$		
$I^\pi$	$E_{\text{ex}}$	$E_{\text{th2}}$	$I^\pi$	$E_{\text{ex}}$	$E_{\text{th2}}$	$I^\pi$	$E_{\text{ex}}$	$E_{\text{th2}}$
(g.b)			(g.b)			(g.b)		
$2^+$	0.155	0.159	$2^+$	0.163	0.165	$2^+$	0.192	0.198
$4^+$	0.419	0.442	$4^+$	0.436	0.453	$4^+$	0.490	0.514
$6^+$	0.774	0.804	$6^+$	0.798	0.817	$6^+$	0.877	0.902
$8^+$	1.205	1.226	$8^+$	1.230	1.240	$8^+$	1.342	1.346
$10^+$	1.698	1.696	$10^+$	1.707	1.710	$10^+$	1.857	1.835
$12^+$	2.242	2.207	$12^+$	2.204	2.221	$12^+$	2.336	2.362
$14^+$	2.832	2.754	$14^+$	2.726	2.767			
$16^+$	3.461	3.334						
(s.b)			(s.b)			(s.b)		
$18^+$	4.095	4.112	$16^+$	3.282	3.313	$14^+$	2.825	2.823
$20^+$	4.730	4.720	$18^+$	3.869	3.862	$16^+$	3.394	3.401
$22^+$	5.405	5.391	$20^+$	4.493	4.475	$18^+$	4.051	4.055
$24^+$	6.129	6.124	$22^+$	5.167	5.150	$20^+$	4.788	4.783
$26^+$	6.907	6.919	$24^+$	5.897	5.888	$22^+$	5.597	5.585
			$26^+$	6.686	6.688	$24^+$	6.463	6.463
			$28^+$	7.535	7.552	$26^+$	7.407	7.415

Method 2 is the variable moment of inertia (VMI)

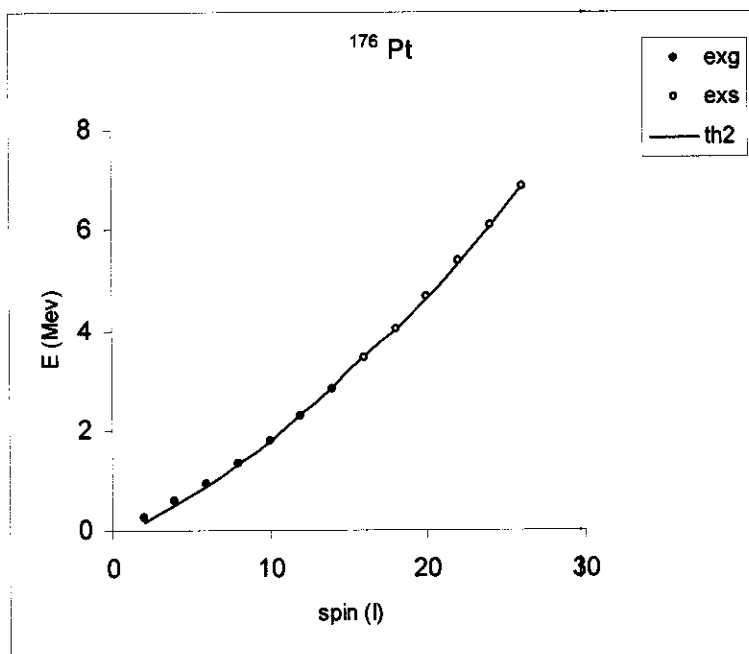


Fig.(4)

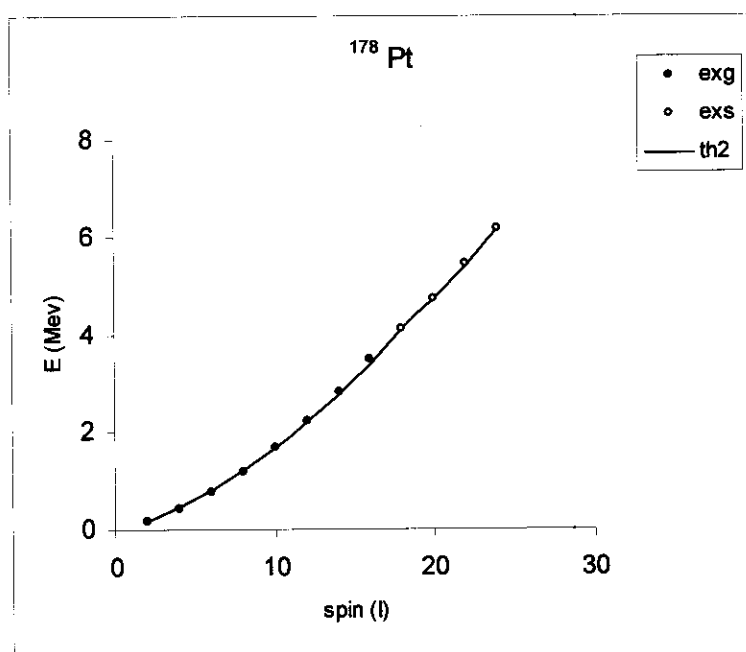


Fig.(5)

Fig. 4, 5 : Plot of the level excitation energies (yrast sequences ) as a function of spin for  $^{176}\text{Pt}$ ,  $^{178}\text{Pt}$  by (method 2).

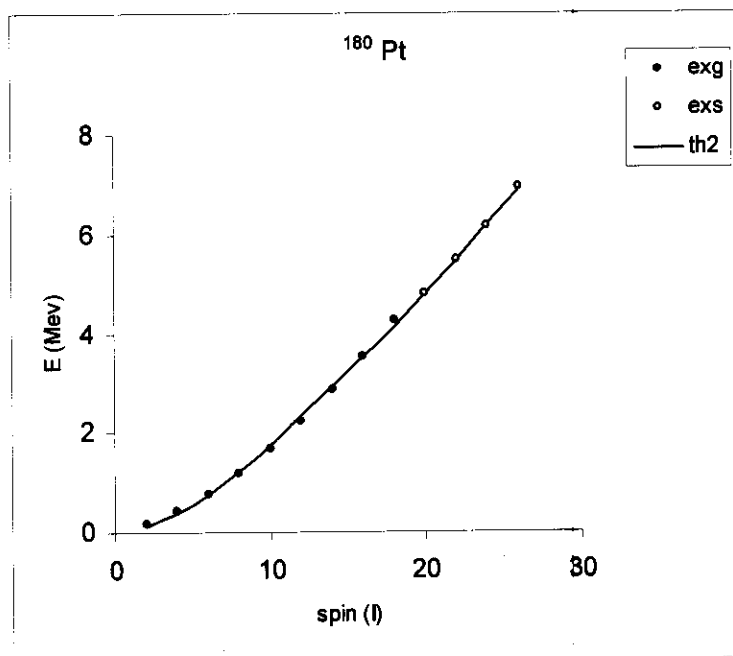


Fig.(6)

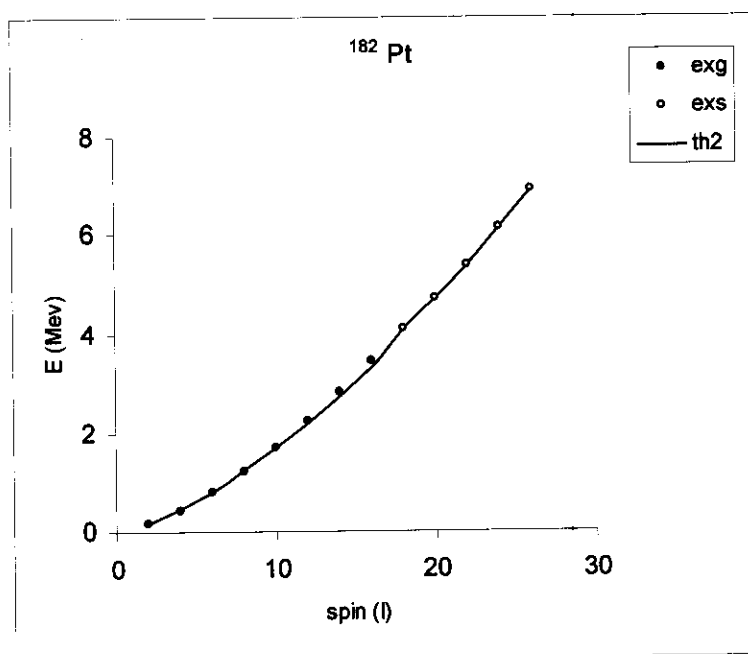


Fig.(7)

**Fig. 6, 7 :** Plot of the level excitation energies (yrast sequences ) as a function of spin for  $^{180}\text{Pt}$ ,  $^{182}\text{Pt}$  by (method 2).

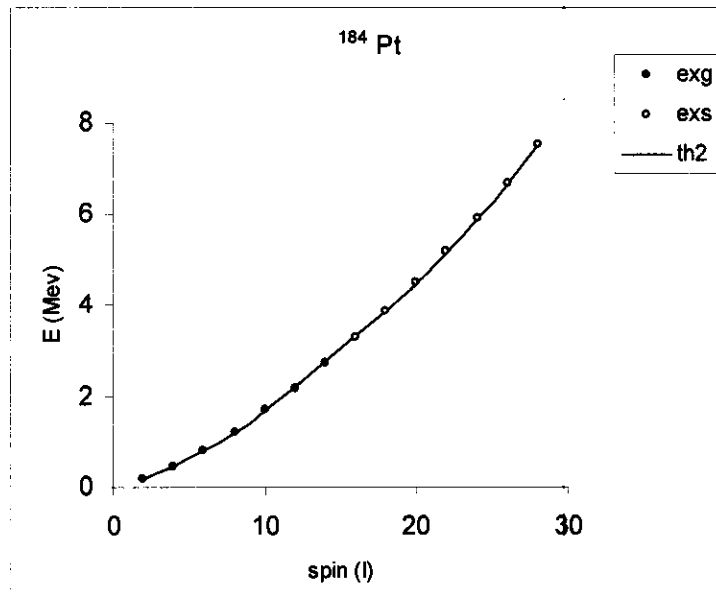


Fig.(8)

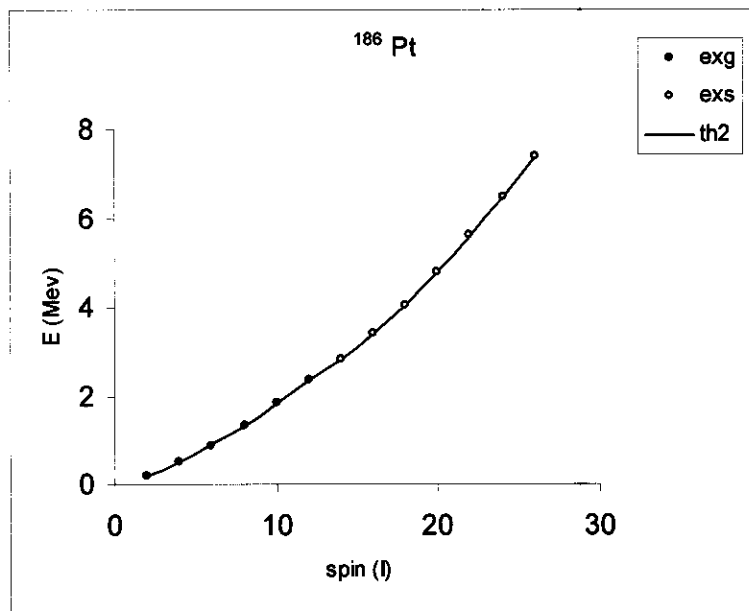


Fig.(9)

**Fig. 8, 9 :** Plot of the level excitation energies (yrast sequences ) as a function of spin for  $^{184}\text{Pt}$ ,  $^{186}\text{Pt}$  by (method 2).